Hyperspectral chemical imaging reveals spatially varied degradation of polycarbonate urethane (PCU) biomaterials

Dorrepaal, Ronan M; Lawless, Bernard M; Burton, Hanna E; Espino, Daniel M; Shepherd, Duncan E T; Gowen, Aoife A

DOI:
10.1016/j.actbio.2018.03.045

Hyperspectral chemical imaging reveals spatially varied degradation of polycarbonate urethane (PCU) biomaterials

Ronan M. Dorrepaal[1,†], Bernard M. Lawless[2,†], Hanna E. Burton[2,3], Daniel M. Espino[2], Duncan E.T. Shepherd[2], Aoife A. Gowen[1,*]

[1] UCD School of Biosystems and Food Engineering, University College Dublin, Ireland

[2] Department of Mechanical Engineering, School of Engineering, University of Birmingham, United Kingdom

[3] PDR – International Centre for Design and Research, Cardiff Metropolitan University, United Kingdom

[†]These authors contributed equally to this study

*Corresponding author: Email: aoife.gowen@ucd.ie

Tel: +353 1 716 2601 Fax: +353 1 716 7415

Abstract

Hyperspectral chemical imaging (HCI) is an emerging technique which combines spectroscopy with imaging. Unlike traditional point spectroscopy, which is used in the majority of polymer biomaterial degradation studies, HCI enables the acquisition of spatially localised spectra across the surface of a material in an objective manner. Here, we demonstrate that attenuated total reflectance Fourier transform infra-red (ATR-FTIR) HCI reveals spatial variation in the degradation of implantable polycarbonate urethane (PCU) biomaterials. It is also shown that HCI can detect possible defects in biomaterial formulation or specimen production; these spatially resolved images reveal regional or scattered spatial heterogeneity. Further, we demonstrate a map sampling method, which can be used in time-sensitive scenarios, allowing for the investigation of degradation across a larger component or component area. Unlike imaging, mapping does not produce a contiguous image, yet grants an insight into the spatial heterogeneity of the biomaterial across a larger area. These novel applications of HCI demonstrate its ability to assist in the detection of defective manufacturing components and lead to a deeper understanding of how a biomaterial's chemical structure changes due to implantation.

Keywords: Biomaterial characterisation, biostability, hyperspectral chemical imaging, *in vivo* degradation, polycarbonate urethane.

1. Introduction

A biomaterial is a material intended to interface with biological systems to evaluate, treat, augment or replace any tissue, organ or function of the body [1]. The human body is an aggressive environment for biomaterials [2] and may have an adverse effect on the performance of these materials [3]. To gain an understanding of the failure mechanisms associated with the *in vivo* performance of an implanted device (and its biomaterial components), it is important to examine explanted (retrieved) devices [4]. Mechanical wear and damage characterisation are important in retrieval analysis studies, however, investigations relating to changes to chemical structure due to the biological environment are equally necessary [4]. Long-term implantable polymers are an important class of biomaterials, used in a variety of biomedical applications [5]. In particular, the polyurethane (PU) group, and more specifically polycarbonate urethanes (PCU), are used in vascular catheters [6,7] and orthopaedic [8–11] applications. Though PCU has been shown to be more biostable than polyether urethanes (PEU) [12,13], another polymer in the PU group used in cardiovascular applications [14], PCU components of explanted orthopaedic implants have been reported to degrade in the human body due to oxidation [9,15]. This oxidative degradation results in the cleavage of chemical bonds in a polymer [16] and has been shown to adversely affect the surface chemical structure of the PCU spacer of the Dynesys spinal stabilisation device (Zimmer, Warsaw, Indiana, USA) [9,15,17,18]. To replicate and understand the effect of *in vivo* oxidation on chemical structure, an accelerated *in vitro* oxidation method to degrade PCU biomaterials has been reported [8,12,19]. This process produces hydroxyl radicals from the $H_2O_2/CoCl_2$ solution and is reported to be an appropriate model of the *in vivo* processes which produce oxygen radicals

at the polymer/cell interface [20]. By using this *in vitro* degradation method, it was shown that oxidative degradation also affects the viscoelastic properties of the BDyn spinal stabilisation device (S14 Implants, Pessac, France), and its components, at specific frequencies [8].

Fourier transform infra-red (FTIR) spectroscopy is one of the three recommended techniques to quantify the chemical structure of polymers according to the ISO standard 10993-18, in addition to nuclear magnetic resonance (NMR) spectroscopy and mass spectroscopy (MS). Attenuated total reflectance Fourier transform infra-red (ATR-FTIR) spectroscopy has been used to understand and characterise the chemical structure changes of films [12,19,21–23], tubing [21], dumbbell or cylindrical specimen shapes [24–28], pacemaker or defibrillator leads [14,29] and orthopaedic devices [8,9,15,17,18]. A major limitation of standard ATR-FTIR, as conventionally applied, is that spectra are usually acquired from a single point of a sample. This risks missing critical information of how, and the extent to which, degradation varies across an explant spatially, as well as potential operator bias in the selection of an acquisition point on an explanted component. To overcome these potential risks, the acquisition of spatially resolved chemical data is desirable. Hyperspectral chemical imaging (HCI) is an emerging technique which combines spectroscopy with imaging, enabling the acquisition of spatially localised spectra across the surface of a material [30,31]. The feasibility of mid-infrared HCI has been demonstrated for high-throughput, non-destructive monitoring of biochemical processes directly at the cellular level [32], evaluation of the molecular state of polymer matrices for drug release [33] and protein adsorption on monolayers [34]. ATR-FTIR HCI enables the acquisition of spectra from the surface of samples that would otherwise be too thick for conventional mid-

IR spectroscopy. A tutorial on the acquisition of hyperspectral chemical images and subsequent computational analysis (through both Matlab and R) has been previously presented [35]. However, to the best of the authors' knowledge, the potential of this technique for evaluation of surface variations in the degradation of long-term implantable biomaterials has not been evaluated. Here, we demonstrate that ATR-FTIR HCI reveals spatial variations in the degradation of polymer biomaterials. Two long-term implantable PCUs (Bionate II 80A and ChronoFlex C 80A) were degraded by two different *in vitro* oxidation methods. Comparisons, based on HCI data, were made between the untreated specimens and specimens degraded through *in vitro* oxidation. Further, this study investigated and reports variations of the *in vivo* degradation of an explanted biomaterial component from an orthopaedic device using HCI.

2. Materials and methods

2.1 Biomaterials

Bionate II 80A (DSM, Heerlen, Netherlands) and ChronoFlex C 80A (AdvanSource Biomaterials, Wilmington, MA, USA) are commercially available long term implantable polycarbonate urethane (PCU) biomaterials. These were gathered in pellet form and injection moulded into 150 mm x 150 mm sized plaques [36] with a thickness of 3 mm ± 0.2 mm according to the individual manufacturers' recommendations. As per implantation protocols, the plaques were sterilised by Ethylene Oxide (EtO) (Steriservices, Bernay, France). This process involves three cycles with an EtO concentration of 600 mg/L for 4 hours at 43 °C. No separate aeration was implemented as aeration was performed in the chamber. The plaques were then cut into the defined ASTM D1708 specimen shape [37] by using a die cutter (Wallace Instruments, Cambridge, UK) on a Wallace Hand Operated

Specimen Cutting Press (Wallace Instruments, Cambridge, UK). From each plaque, 23 specimens were cut. Once a plaque was cut, the specimens were numbered and a random order generator (Excel 2010, Microsoft, Redmond, Washington, USA) was used to separate the specimens into untreated (n=6), 3% H_2O_2 (n=6) and 20% H_2O_2 / 0.1*M* (n=6) groups.

2.2 *In vitro* degradation of biomaterials

30% hydrogen peroxide (H_2O_2) Fisher Scientific, Loughborough, United Kingdom) and 0.1*M* cobalt (II) chloride hexahydrate ($CoCl_2.6H_2O$) (Sigma Aldrich, Dorset, United Kingdom) were used in the preparation of the oxidative degradation solutions. The 30% H_2O_2 was diluted to the appropriate 3% H_2O_2 and 20% H_2O_2 concentration levels using deionized water [13].

The ISO 10993-13 method was followed to degrade Bionate II 80A and ChronoFlex C 80A with 3% H_2O_2. Oxidative degradation of the biomaterials was performed at 37°C ± 1°C in a water bath (JB5 Water Bath, Grant Instruments, Cambridgeshire, United Kingdom). The solution was changed every seven days and the degradation period was 52 weeks. The solution did not include any metal ions to catalyse the decomposition of the hydrogen peroxide [24]. After the degradation period, the specimens were rinsed with deionised water and dried under vacuum for 48 hours at room temperature.

The commonly used accelerated oxidation method [8,12,19] was also used to degrade the PCU biomaterials with 20% H_2O_2/0.1*M* $CoCl_2.6H_2O$. To maintain a relatively constant concentration of radicals [19], the H_2O_2/$CoCl_2.6H_2O$ solution was changed every three days while the degradation period lasted 24 days. Similar to the ISO 10993 method, accelerated oxidative degradation was performed at 37°C ± 1°C in a water bath (JBN18 Water Bath, Grant Instruments, Cambridgeshire, United Kingdom). After the degradation period, the

specimens were rinsed with deionised water and were dried under vacuum for 48 hours at room temperature.

2.3 BDyn Posterior Dynamic Stabilisation device

The BDyn Posterior Dynamic Stabilisation (PDS) device (S14 Implants, Pessac, France) is a bilateral system designed to preserve intersegmental range of motion, reduce intradiscal pressure and alleviate loading of the facet joints [11]. It comprises of a polycarbonate urethane ring (Bionate II 80A, DSM, Heerlen, The Netherlands) and a silicone cushion (MED-4770, NuSil Technology LLC, Carpinteria, CA, USA), a mobile titanium alloy rod, a fixed titanium alloy rod and is fixed to the vertebrae by titanium alloy pedicle screws [11]. The BDyn explant was sent to S14 Implants (Pessac, France) after complications with the device. The titanium alloy housing was carefully cut along a laser weld to expose the PCU and silicone components and the components were sterilised. Patient details were unobtainable, however, the estimated implantation time (based on distribution of implants to retrieval surgery date) was approximately six months.

2.4 Hyperspectral Chemical Imaging

A Thermo Scientific™ Nicolet™ iN™10 Infrared Microscope (10× magnification, Mercury-Cadmium-Tellurium (MCT) detector, working range 4000-675 cm^{-1} with a 2 cm^{-1} spectral resolution) was used in combination with a slide-on Germanium ATR Micro Tip to collect ATR-FTIR hyperspectral chemical images. The system was nitrogen gas purged for an hour before use and the purge was maintained during use. The detector was a liquid nitrogen cooled and allowed to equilibrate for an hour before use. This was also maintained during acquisition. Specimens were attached to glass slides and inserted into the instrument. A white light mosaic image was collected to aid with hyperspectral collection.

2.4.1 Imaging of *in vitro* degraded biomaterials

A detector aperture size of 200 µm was selected, and the resultant spatial resolution of the ATR Micro Tip using the single point detector was 50 µm. After selecting a region of interest in the centre of each biomaterial sample, grids of data points were selected such that the distance between each pixel was 50 µm, in order to generate spatially contiguous images. Pixel acquisition time was ~11.2 seconds and images were 1296 pixels in size resulting in a total acquisition time of ~4 hours (typically the collective acquisition times of x spectra will be approximately x times longer than the collection of a single spectrum).

2.4.2 Imaging of *in vivo* degraded explant

An aperture size of 150 µm was selected, and the resultant spatial resolution of the ATR Micro Tip using the single point detector was 37.5 µm. After selecting a region of interest in the explant specimen, a grid of data points was selected such that the distance between each pixel was 100 µm, in order to generate a spatially resolved (non-contiguous) hyperspectral chemical map.

2.4.3 Raman mapping

In order to independently corroborate the ATR-FTIR results, identical areas of Bionate II 80A materials were analysed using both ATR-FTIR and Raman spectroscopy mapping. These materials were from the same experimental batch as the *in vitro* studies described above in section 2.2 but were examined 6 months after the original experimental protocol and after subsequent mechanical testing of the samples.

Raman maps were acquired using an inVia Micro-Raman confocal spectroscopy system (Renishaw, Wotton-under-Edge, Gloucestershire, UK) with a 10x 0.25NA objective lens, 785

nm edge laser (laser power was 306 mW at source, and was set to 1% power for sample measurements) and an 600 line mm^{-1} grating without pinhole. Spectra were calibrated to a silicon shift at 520 cm^{-1}. The detector used was a NIR enhanced Deep Depletion CCD array (1024 × 256 pixels) which was Peltier cooled to -70°C. The spectral range was 3035.3 cm^{-1} - 1089.1 cm^{-1} with a mean spectral resolution of 1.9231 cm^{-1} over 1013 measured spectral bands. As contiguous Raman imaging over a similar area to the ATR images was not feasible within a reasonable timeframe, areas were mapped rather than imaged (using a step size of 15 µm). The laser footprint was rectangular/oval in shape, with the longer dimension mapping to the vertical direction of the generated Raman map. As the step size was equal in X and Y directions, this resulted in a vertically directed elongated appearance in features of the Raman images.

ATR-FTIR imaging parameters were as described in section 2.4.1.

2.5 Pre-processing

ATR-FTIR spectra were pre-processed as described below. The spectral range was cut to 2000 cm^{-1} - 675 cm^{-1}. The spectra were then scaled to a stable aromatic C-H out of plane bending peak at 819 cm^{-1} [9]. Linear baseline correction was subsequently performed and followed by a baseline shift of one arbitrary unit. A peak at ~1591-1596 cm^{-1} indicative of C=C bond stretching of an aromatic ring of the hard segment [12,21,23,38] has been reported to remain unchanged in PCU oxidation [39], and has therefore been used as internal reference peak in the literature. However such an approach is not suitable in the present instance as a neighbouring peak overlaps the C=C stretching peak and consistency of its intensity between spectra cannot be assumed. In other studies PCU spectra have been

normalised to an aromatic internal reference peak at 508 cm^{-1} [4], however this was outside of the measured range.

Internal normalisation was not possible in the case of the *in vivo* specimen image due to the disappearance of the 819 cm^{-1} peak in highly degraded regions. For this reason, SNV normalisation (spectrum-wise mean subtraction with spectrum-wise division by standard deviation) was used in the case of the *in vivo* image.

No pre-processing was applied to the Raman spectra.

2.6 Data analysis

The mean spectrum was calculated for each image and randomised sample spectra were inspected. Randomisation was achieved through the "rand" function of Matlab. Histograms were produced at wavenumbers of interest in order to assess the shape of absorbance distributions. ATR images at particular wavenumbers of interest were inspected.

Peak ratio images were also generated. The ratio between peaks reported to be indicative of degradation (1650 cm^{-1} (growing): aromatic amine and 1248 cm^{-1} (shrinking): carbonate [12,17,21]) were calculated and resultant dimensionless ratio value images were generated. Trends in these images were compared to the trends of the single wavenumber images.

The "parula" (blue → green → yellow) colour scale was used for the image generation of all *in vitro* images as this colour scale ranges from dark to bright incrementally. This is an important consideration as colour scales which do not possess this property can result in human error when arbitrary dramatic colour changes cause the observer to believe a greater difference exists than is actually the case. The "hot" colour scale was used in all

overlaid *in vivo* maps as this colour scale increments from dark to bright but also contrasts well with the white-light image onto which it has been overlaid.

Multivariate analysis was conducted in relation to *in vitro* specimens only. Reference spectra were chosen to represent both degraded and undegraded materials. The mean control spectrum (B0) was chosen as an undegraded reference spectrum, while the mean spectrum of the material exposed to the harshest oxidation technique (B20) was chosen as a degraded reference spectrum. The undegraded reference spectrum was then subtracted from the degraded reference spectrum to produce a difference spectrum which highlights features associated with degradation. Each HCI (B0, B3 and B20 *in vitro* Bionate II 80A images) was then projected along the difference spectrum, by multiplying the HCI spectra by the difference spectrum, and converting each pixel-spectrum to a single index representative of the level of degradation. A histogram was produced to assess the distribution of these indices and to select threshold points for separation of groups of pixels into classes according to degradation level. Finally, the degradation classes were visualised as images and the mean spectrum of each class was inspected. The time taken to process the data (including initial loading and image generation) was 28.5seconds, on Windows 10 running Matlab 2017b.

2.7 Statistical analysis

Each HCI comprised 1296 spectra. Descriptive statistics, i.e. the sample means and standard deviations of the intensities of the peaks of interest (1174 cm^{-1}, 1248 cm^{-1} and 1650 cm^{-1}) were calculated from each image.

3. Results

3.1 Univariate analysis of Bionate II (*in vitro* degradation)

The mean spectra of the hyperspectral chemical images of control (B0), 3% H_2O_2 (B3) and 20% H_2O_2/0.1*M* $CoCl_2.6H_2O$ (B20) treatments for Bionate II 80A (DSM, Heerlen, Netherlands) were calculated (Fig. 1). As reported in the literature [12,17,21] 1174 cm^{-1} is indicative of C-C cross-linking, 1248 cm^{-1} is indicative of C-O-C carbonate bonds, and 1650 cm^{-1} is indicative of aromatic amines (Supplementary Table 1). It was found that little to no C-C cross-linking peak exists at 1174 cm^{-1} in the mean spectra of the B0 and B3 specimens, while a small yet notable peak emerges in the B20 specimen mean spectrum. Further, it is evident that the carbonate peak at 1248 cm^{-1} decreased in the B20 specimen relative to the B0 and B3 specimens, suggesting degradation of the carbonate soft segment. Finally, no aromatic amine peak or band was detected at 1650 cm^{-1} in the mean spectra of B0 and B3, however, a subtle band is visible in the B20 mean spectrum.

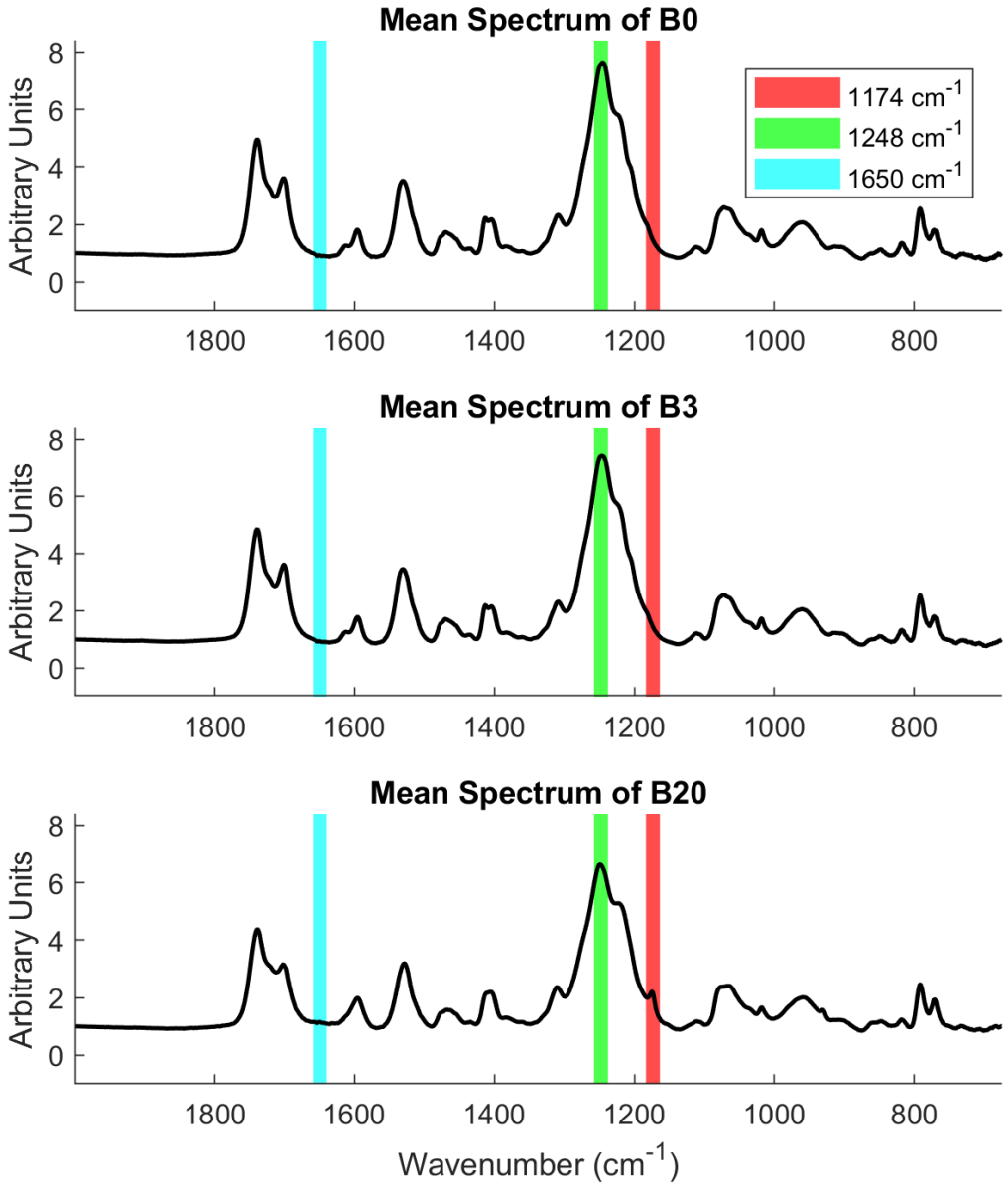

Figure 1. Image mean spectra of B0 (top), B3 (middle) and B20 (bottom) for Bionate II 80A. Colour bars have been added to indicate the spectral ranges associated with polycarbonate urethane degradation (1174 cm^{-1} [range: 1183 cm^{-1} to 1160 cm^{-1}]: C-C cross-linking, 1248 cm^{-1} [range: 1260 cm^{-1} to 1235 cm^{-1}]: C-O-C carbonate, and 1650 cm^{-1} [range: 1662 cm^{-1} to 1630 cm^{-1}]: aromatic amine) (Supplementary Table 1).

To inspect whether the mean spectrum is an accurate representation of each specimen, 100 spectra were randomly selected from each hyperspectral chemical image (Fig. 2). While B0

and B3 show little variability between spectra (and their corresponding mean spectra shown in Fig. 1), this is not the case for the B20 spectra which exhibit considerable variability within the sample, particularly in the case of the aromatic amine peak at 1650 cm^{-1} and the carbonate peak at 1248 cm^{-1}.

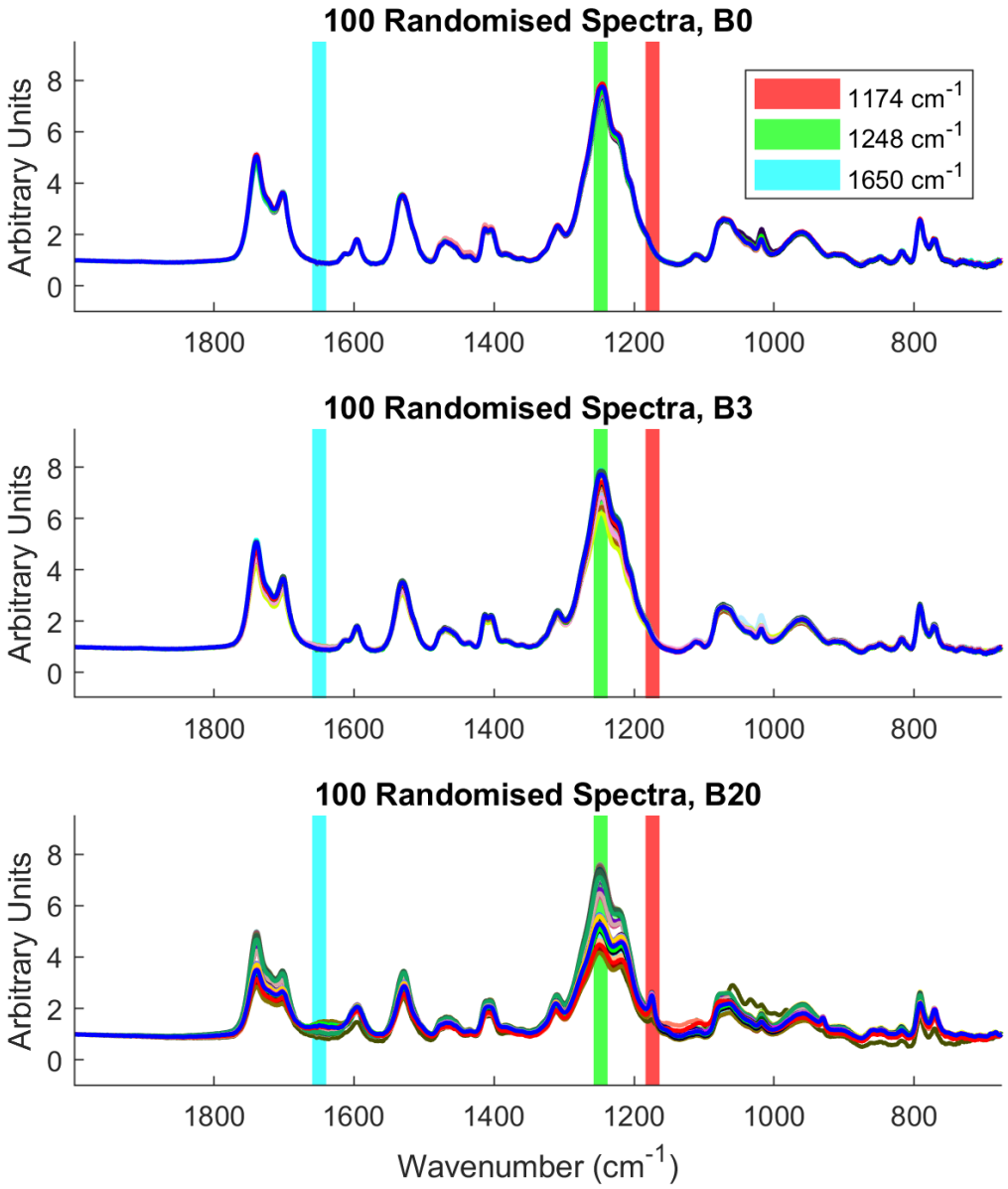

Figure 2. 100 randomised spectra from hyperspectral chemical image of B0 (top), B3 (middle) and B20 (bottom) for Bionate II 80A. Colour bars have been added to indicate the spectral ranges associated with polycarbonate urethane degradation (1174 cm^{-1} [range: 1183 cm^{-1} to 1160 cm^{-1}]: C-C cross-linking, 1248 cm^{-1}

[range: 1260 cm^{-1} to 1235 cm^{-1}]: C-O-C carbonate, and 1650 cm^{-1} [range: 1662 cm^{-1} to 1630 cm^{-1}]: aromatic amine).

To further investigate heterogeneities in each sample, single wavenumber images were generated at the wavenumbers reported to be related to degradation [12,24], accompanied by corresponding histograms (Fig. 3, Supplementary Fig. 1 and Supplementary Fig. 2). From visual inspection, no C-C cross-linking (at 1174 cm^{-1}) was detected in the B0 and B3 images (Fig. 3). However, the entire imaged surface of the B20 specimen has experienced C-C cross-linking. Interestingly, the degree to which C-C cross-linking has occurred is highly variable. In the case of B0 and B3, the histogram (Fig. 3, bottom right) shows a mono-modal distribution in relation to 1174 cm^{-1}. These distributions appear to substantially overlap, with similar means (1.45 and 1.43) and standard deviations (0.02 and 0.02) for B0 and B3 respectively, while the B20 sample had a larger mean (2.15) and standard deviation (0.19). A bi-modal distribution at 1174 cm^{-1} can be observed in the case of B20, suggesting that there are at least two degradation populations in the B20 specimen. The corresponding B20 image (Fig. 3, bottom left) reveals the spatial arrangement of these degradation populations.

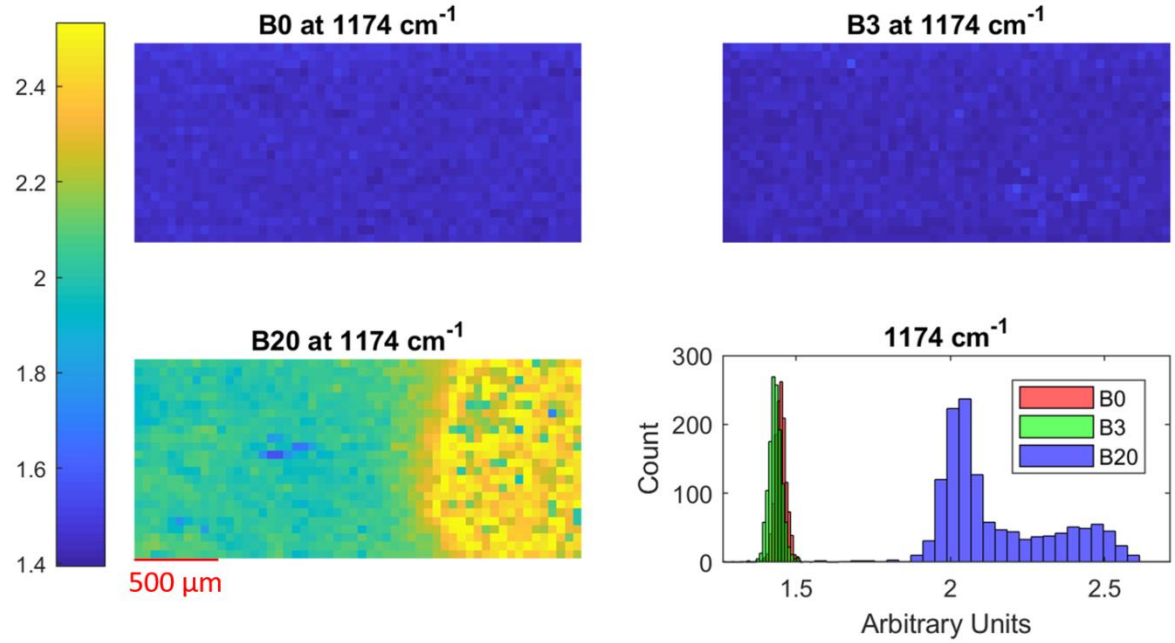

Figure 3. Images of B0 (top left), B3 (top right) and B20 (bottom left), with accompanying histogram (bottom right) depicting relative absorbance at 1174 cm^{-1}. Image colour scale from 1st to 99th percentile.

The distribution of the 1248 cm^{-1} carbonate peak varied across the surface of all samples (Supplementary Fig. 1). The histogram demonstrates a mono-modal distribution in the case of both B0 and B3, which have similar means (7.58 and 7.42) and similar standard deviations (0.18 and 0.20), while B20 has in this case a smaller mean (6.61) and larger standard deviation (1.08). Once again, in the case of B20, a bi-modal distribution is visible in the histogram (Supplementary Fig. 1, bottom right) which is spatially resolved in the accompanying image (Supplementary Fig. 1, bottom left). While, from the histogram, it appears that there is a mono-modal 1248 cm^{-1} distribution in the case of B0 and B3, several pixels of their corresponding 1248 cm^{-1} images (Supplementary Fig. 1, top left and right respectively) appear to be of lower intensity than the majority, suggesting small scattered regions of carbonate soft segment degradation. These regions are not clearly distinguishable in the histogram due to their scarcity. Equivalently, left and central regions of the B20 1248

cm^{-1} image (Supplementary Fig. 1, bottom left) comprise pixels of considerably higher intensity (brighter pixels) than the image mean, suggesting a lack of carbonate degradation in this region. An emerging peak at 1650 cm^{-1}, associated with the formation of aromatic amines, is generally indicative of hard segment degradation [12,24] (Supplementary Fig. 2). As before, upon inspection of the histogram (Supplementary Fig. 2, bottom right), B0 and B3 can be described as comprising a mono-modal distribution (again with similar means (0.93 and 0.94) and standard deviations (0.03 and 0.04)) and B20 can be seen to comprise a bi-modal distribution with a mean of 1.15 and standard deviation of 0.16 (Supplementary Fig. 2). Similar to the 1248 cm^{-1} images, the 1650 cm^{-1} images are not homogeneous, with apparent outlier pixels visible in all three specimen images at the same positions as those of the 1248 cm^{-1} images.

To further investigate the apparent outlier pixels of the single wavenumber images, individual pixels were selected from the 1650 cm^{-1} images and their associated spectra were visualised to assess their chemical differences (Fig. 4).

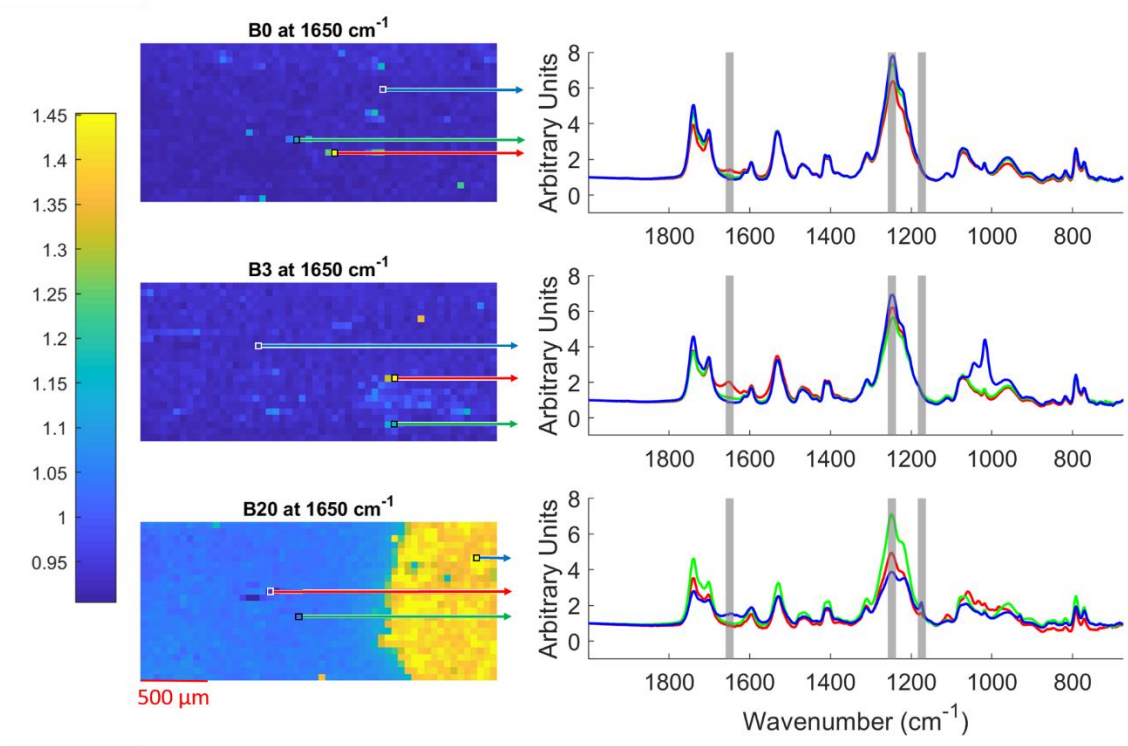

Figure 4. Spectra of pixels selected from images of relative absorbance at 1650 cm^{-1} for B0, B3 and B20.All images scaled equally (height and width). Image colour scale from 1st to 99th percentile.

It can be seen that bright pixels indicate the presence of a greater 1650 cm^{-1} absorbance intensity in the associated spectrum, while the darker pixels indicate a lower absorbance intensity at the 1650 cm^{-1} position. Observation of the selected spectra indicates they are not truly outliers (e.g. due to errors in detection), but rather represent highly localised specimen regions with different chemical features. Cell-biomaterial interactions in these regions could vary significantly from the un-degraded surface regions, resulting in potential complications with an implant. For example, regions of degradation could act as sites for protein adhesion, leading to issues such as biofilm formation. Similar spatial features are evident when comparing the 1650 cm^{-1} images to the dimensionless peak ratio images (Supplementary Figures 3 and 4). In these peak ratio images, the same pixel intensity trends were observed regardless of normalisation.

Raman hyperspectral chemical maps were compared with ATR-FTIR HCIs as a means of independent corroboration of the results. Supplementary Figures 5 (B0) and 6 (B20) present mean Raman images, and ATR-FTIR images at 1650 cm^{-1}. Changes in measured fluorescence appeared to be a major cause of the differences observed between Raman pixels. It should also be noted that features which are IR active are not equivalently active in the case of Raman spectroscopy, leading to changes in relative intensity of pixel features between modalities. Furthermore, the Raman laser footprint is considerably smaller than the ATR-FTIR detection area. Therefore smaller features could be resolved by this technique. Nevertheless, similar pixel patterns, indicating spatially varying degradation, were detected with both modalities, thus corroborating the observed results.

3.2 Univariate analysis of ChronoFlex C (*in vitro* degradation)

Similar observations were made in relation to other PCU biomaterials, specifically ChronoFlex C 80A (AdvanSource Biomaterials, Wilmington, MA, USA). The HCI mean spectrum of a ChronoFlex C 80A specimen subjected to the B20 oxidation method, appears to show a subtle aromatic amine peak at 1650 cm^{-1} as well as a C-C cross-linking peak at 1174 cm^{-1} (Supplementary Fig. 7, top). The peak at 1248 cm^{-1} may have reduced in relative intensity, however, this is difficult to determine from a single mean spectrum. When 100 randomised spectra were assessed (Supplementary Fig. 7, bottom), it was found that the 1248 cm^{-1} intensity varied considerably. To assess the pixel intensity distributions for the wavenumbers of interest, single wavenumber histograms (at 1174 cm^{-1}, 1248 cm^{-1} and 1650 cm^{-1}) were generated (Supplementary Fig. 8). The corresponding single wavenumber images present the spatial arrangements of these intensity distributions (Supplementary Fig. 8). It

can be seen that, like the Bionate II 80A specimen subjected to the B20 method, there is considerable variation in the levels of material degradation detected within the sample.

3.3 Univariate analysis of Bionate II (*in vivo* degradation)

ATR mapping was also applied to a PCU component (Supplementary Fig. 9) (Bionate II 80A, DSM, Heerlen, Netherlands) explanted from a BDyn device. Mapping of *in vivo* specimens provides a unique insight into the authenticity of *in vitro* oxidation methods, particularly with respect to the spatial heterogeneity of degradation. The selected area of the PCU ring component (Supplementary Fig. 10) was magnified with 1174 cm^{-1}, 1248 cm^{-1} and 1650 cm^{-1} single wavenumber colour maps overlaid (Fig. 5). Each map was acquired by defining an acquisition matrix with regularly spaced acquisition points, where the acquistion step size was larger than the detector aperture size. While such a method does not result in a spatially contiguous image, it does allow for the spectroscopic assessment of larger specimen regions, with a relative reduction in acquisition time, allowing for use in time-sensitive studies. The hyperspectral chemical maps revealed that degradation of the *in vivo* specimen is spatially diverse, as was also found with *in vitro* degradation methods. Further, the actual spatial arrangement of the degradation appears to follow a trend with respect to the PCU ring radial position. This was found to be the case for the formation of the aromatic amine peak at 1650 cm^{-1}, the C-C cross-linking peak at 1174 cm^{-1} and the disappearance of the C-O-C carbonate peak found at 1248 cm^{-1} (Fig. 5), all of which are reported identifiers of PCU oxidative degradation. It should be noted that the regions exhibiting 1650 cm^{-1} aromatic amine formation do not perfectly coincide with the presence of 1174 cm^{-1} C-C cross-linking (Fig. 5).

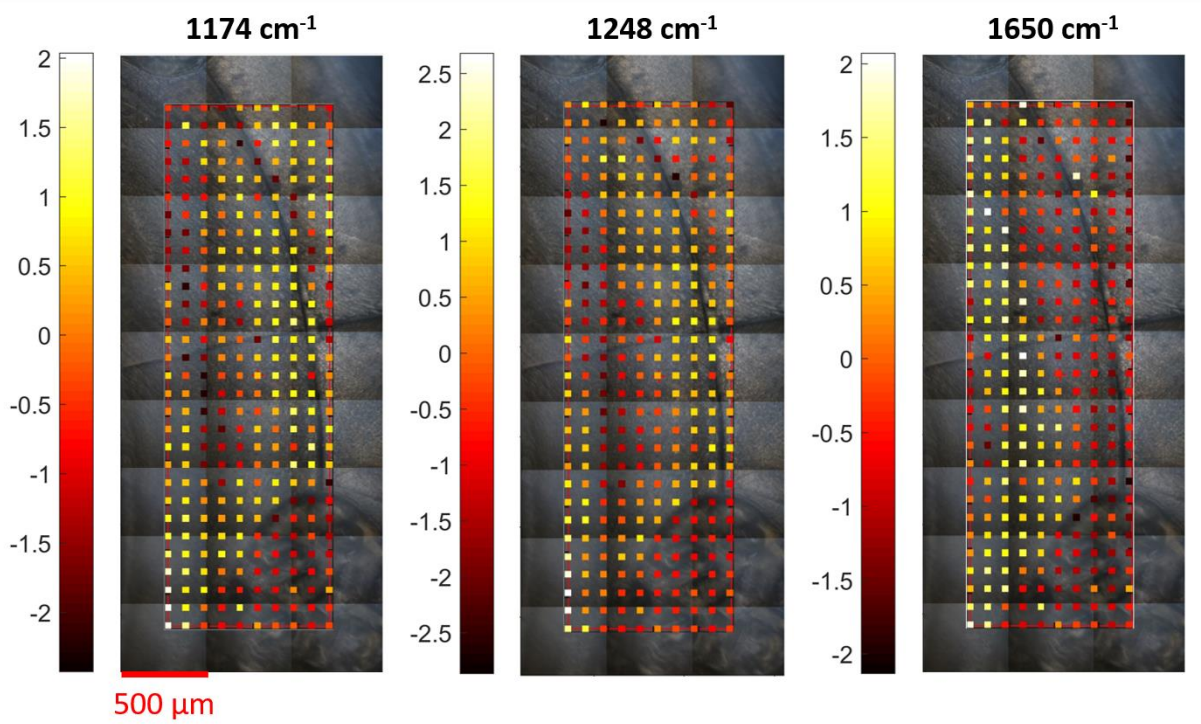

Figure 5. ***In vivo*** **explant with single wavenumber 1174 cm^{-1}, 1248 cm^{-1} and 1650 cm^{-1} maps overlaid. All images scaled equally (height and width).**

3.4 Multivariate analysis (Difference Spectrum Projection)

Multivariate analysis was conducted according to the methodology section. The mean spectra of Bionate II 80A specimens (B0 untreated and B20 treated) are presented (Fig. 6). These spectra were defined as reference undegraded and degraded spectra respectively and were used to calculate a degradation difference spectrum (subtraction of the former from the latter) (Fig. 6). It can be seen that peaks reported in the literature as being indicative of PCU degradation (the emergence of peaks at 1174 cm $^{-1}$ and 1650 cm^{-1}, in addition to the decline of a peak at 1248 cm^{-1}) are highlighted in this degradation difference spectrum by being above or below the baseline as appropriate.

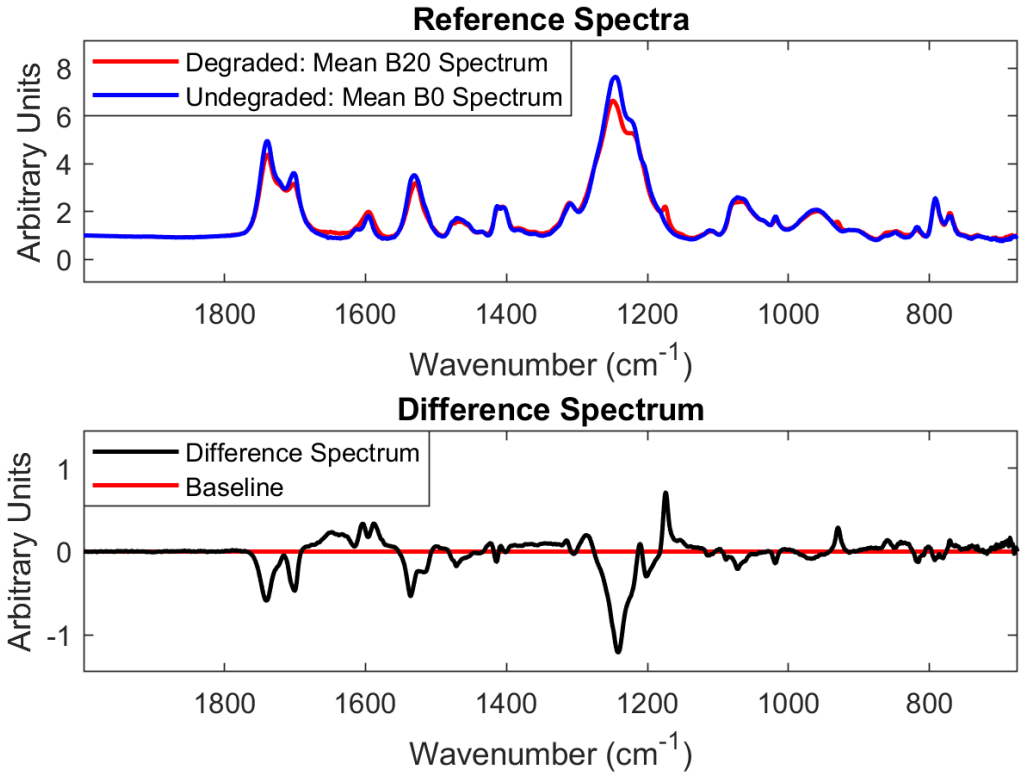

Figure 6. Undegraded and degraded reference spectra (top) and difference spectrum calculated from the subtraction of undegraded reference from degraded reference, including baseline (bottom).

The *in vitro* hyperspectral chemical images were projected along the degradation difference spectrum, which applied weights to each wavenumber according to the difference spectrum in Figure 6 and summed the resultant values. The output values were used to generate degradation index maps (Fig. 7). A histogram was also generated and used to investigate the distribution of the degradation indices across all images. Regions of the histogram (Fig. 7) were thresholded where populations were separable. The mean spectra of all pixels assigned to each class are presented (Fig. 8, bottom right). Through these mean spectra, it was found that the classes represented (1) undegraded, (2) degraded and (3) very degraded regions, identified according to the magnitude of the degradation peaks of interest reported in the literature. Class 1 (undegraded, blue colour in Fig. 8) exhibited a large peak at 1248 cm^{-1} and no peaks at 1650 cm^{-1} and 1174 cm^{-1}. Class 2 (degraded, red colour in Fig. 8)

exhibited a slightly smaller peak at 1248 cm^{-1} , increased absorption at 1650 cm^{-1} and a small but distinctive peak at 1174 cm^{-1}. Class 3 (very degraded, green colour in Fig. 8) exhibited a smaller peak at 1248 cm^{-1} and larger peaks at 1650 cm^{-1} and 1174 cm^{-1} Several pixels representing degradation were found in the control specimen and the specimen exposed to B3 oxidation (see red and green pixels in Figure 8), although more were present in B3 than B0. Conversely, some undegraded pixels were found in the specimen exposed to B20 oxidation.

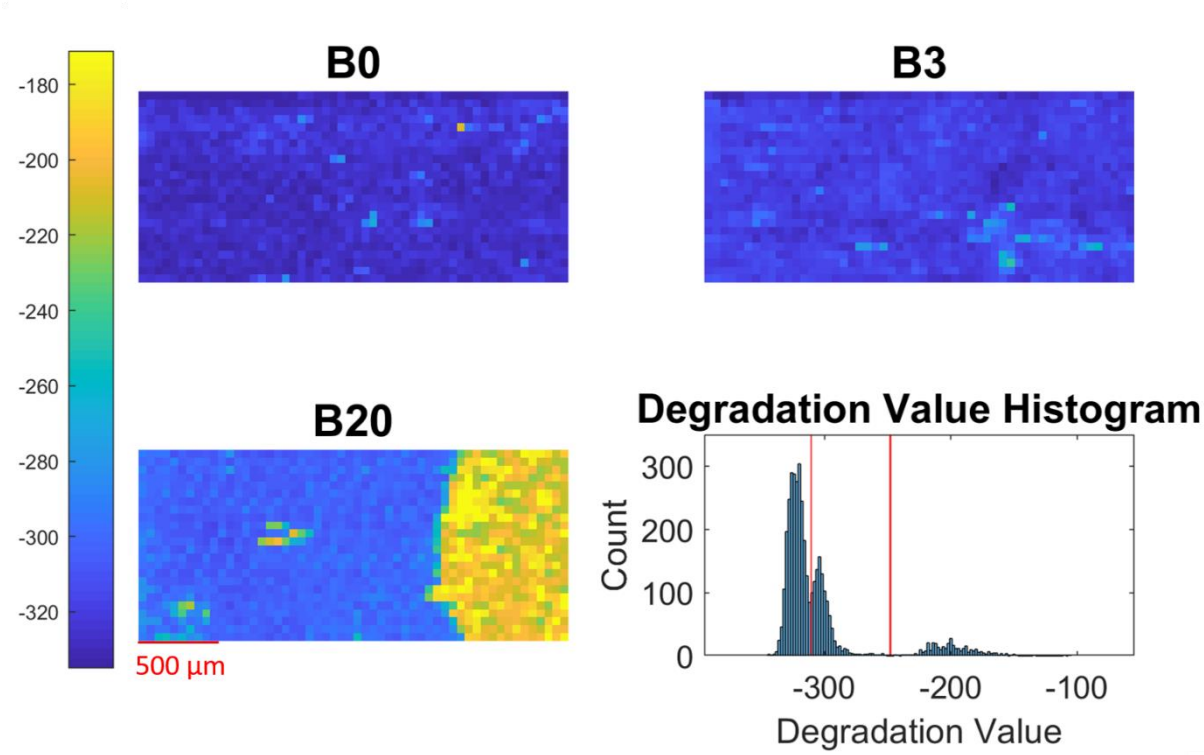

Figure 7. Degradation value images produced by projection of HCIs along degradation difference spectrum, in addition to accompanying histogram. All images scaled equally (height and width). Image colour scale from 1st to 99th percentile. Threshold bars added to histogram.

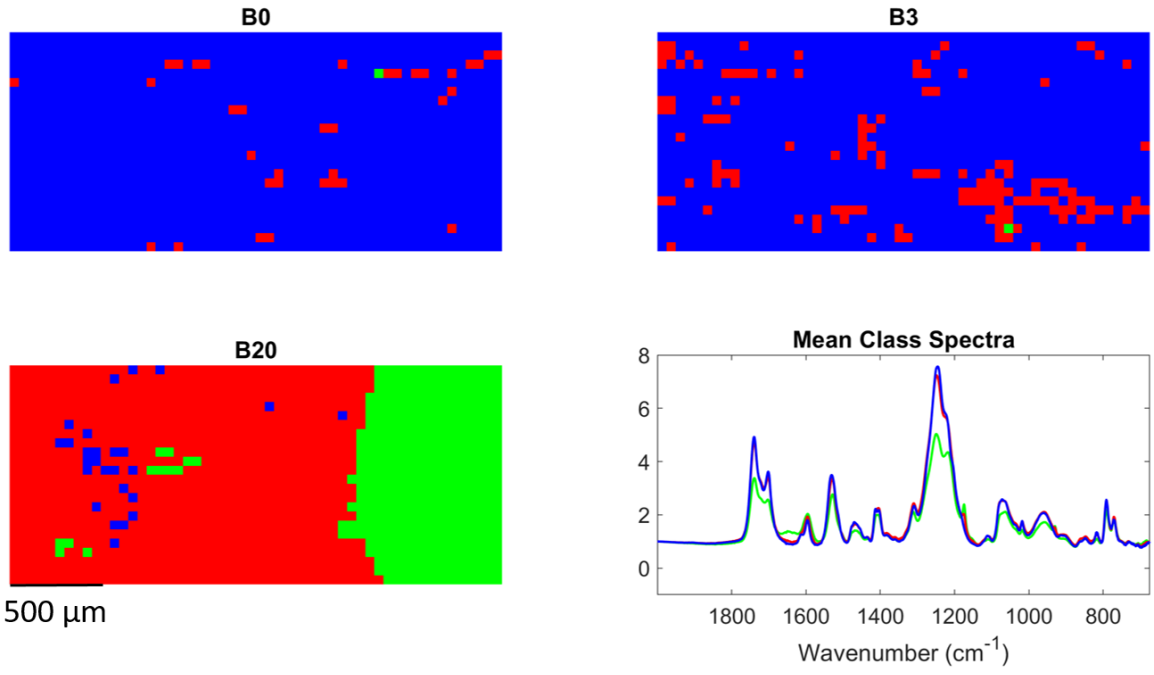

Figure 8. B0, B3 and B20 degradation classification images (top left, top right, bottom left) with colour-coded classification mean spectra (bottom right). All images scaled equally (height and width).

4. Discussion

Through a novel application of HCI, this study demonstrates spatial changes in degradation across PCU biomaterial surfaces. It was found that it is possible to identify regional differences in chemical degradation, allowing for more detailed investigations. The results call into question the validity of the use of traditional point spectroscopic methods by illustrating that, in materials where heterogeneity in surface degradation exists, the acquisition of just one spectrum runs the risk of being unrepresentative of a specimen as a whole. A single spectrum can lead to subjective results as the location of spectral acquisitions can have a large effect on the ultimate conclusions drawn. The present study

has also shown that even in instances where large hyperspectral chemical images are acquired, a single mean spectrum might not represent a material as a whole. Further, a mean spectrum calculated for a large area cannot identify any sub-region of the material, as a mean spectrum is a linear combination of all, possibly very distinct, collected spectra which can result in a "blending" effect. Therefore accurate conclusions can only be drawn from HCI when combined with appropriate data processing techniques. For example, in a previous study which used point acquisition to examine chemical changes, PCUs exposed to 3% H_2O_2 *in vitro* oxidative treatment showed no evidence of hard segment degradation in any of the specimens evaluated [24]. Had point spectroscopy been utilised in the present study, similar conclusions would have been drawn. However it has been demonstrated, through the generation of select wavenumber images [1174cm^{-1}, 1248cm^{-1} and 1650cm^{-1}] and associated histograms, that in some localised regions of the PCU specimen exposed to an identical treatment (B3), a peak emerges at 1650 cm^{-1} (indicating aromatic amine), implying the local occurrence of hard segment degradation [12,24]. Further spatial heterogeneity of degradation was observed in the case of the untreated control specimens (B0) as well as the more harshly oxidised specimens (B20). Without HCI, these chemically distinct regions would go unnoticed, or would be over-represented. The observation of locally distinct chemical regions on the B0 control specimen was unexpected and may have been caused by one or more factors including, potential inconsistencies in the biomaterial mixing/formulation/manufacture process and/or in the sterilisation of the PCU plaques. It may also be caused by mechanical factors. At this time the hard segment changes cannot be attributed to a single factor. Both Trommsdorff et al. [40] and Cipriani et al. [9] stated that, as the degradation is limited to the surface layer, the functionality [40] and the mechanical properties [9] of the entire device are unlikely to be affected. However, Lawless et al. [8]

discovered that the viscous property, of the BDyn device's PCU component, was statistically different, at specific frequencies, after *in vitro* degradation [8].

Ultimately, a balance between efficiency and accuracy should be struck and with that sentiment in mind, hyperspectral chemical mapping was presented with *in vivo* degraded explanted specimens. While such a method does not result in a spatially contiguous image, it does allow for the spectroscopic assessment of larger specimen regions, with a relative reduction in acquisition time, allowing for use in time-sensitive studies. The hyperspectral chemical maps of the *in vivo* degraded PCU component revealed that degradation is spatially diverse; this was also found with *in vitro* degraded PCU specimens. Further, it was discovered that the regions exhibiting 1650 cm^{-1} aromatic amine formation (indicative of hard segment degradation [12,24]) do not perfectly coincide with the presense of 1174 cm^{-1} C-C cross-linking (indicative of soft segment degradation [12,24]) as was found to be the case with *in vitro* degraded specimen, suggesting a more complex degradation mechanism than simple oxidation. In addition, it was observed that degradation heterogeneity appeared to be somewhat radially dependent, possibly due the introduction of localised mechanical stresses or enzyme action. However the cause is not currently known.

Finally, a simple multivariate method was developed coined "difference spectrum projection". This method generated and assigned a degradation index to each pixel of the *in vitro*-degraded PCU biomaterial specimen HCIs. Upon inspection of the degradation index distribution, it was found that the specimens comprise regions drawn from one of three distinct "degradation-level" populations. Despite the use of three different degradation protocols (including one control), heterogeneity in degradation-levels was found across the surface of each specimen, again emphasising the importance of HCI techniques. The

multivariate technique used provides many advantages over standard univariate analysis, not least: significant reductions in operator bias. It should be noted that after reference spectra are selected according to the method, all steps described required can be automated. The difference spectrum generated also has the potential to expose spectral peaks or broad bands which might not be as readily visible to a human operator and is further capable of using multiple identifier peaks in unison.

5. Conclusion

This study demonstrates the potential of hyperspectral chemical imaging (HCI) in the detection of spatial variation of the degradation of PCU biomaterials. The use of HCI can prevent the unavoidable introduction of subjectivity associated with traditional point spectroscopic methods and its use will lead to a deeper understanding of a biomaterial's chemical condition in pre-implantation quality control, *in vitro* degradation studies and retrieval studies. It is proposed that it is now time to move the standard forward, from that of point acquisition to that of HCI.

Acknowledgments

R.M.D. and B.M.L. contributed equally to this work. This study was supported by the European Commission under the 7th Framework Programme (Grant agreement nos.: 604935 and 335508).

Author contributions

R.M.D. and B.M.L. performed hyperspectral chemical imaging of all specimens. B.M.L. and H.E.B. performed all *in vitro* degradation of the polycarbonate urethanes and B.M.L., R.M.D.,

D.M.E. and D.E.T.S. contributed to the design of the degradation experiments. R.M.D. and A.A.G. produced all figures and performed all data analysis within this study. R.M.D., B.M.L. and A.A.G. contributed to the writing of this article. All authors reviewed and edited the manuscript.

Hyperspectral chemical image data, Matlab functions and scripts are available from the authors.

Correspondence and requests should be made to A.A.G.

How to cite this article: Dorrepaal, Lawless *et al*. Hyperspectral chemical imaging reveals spatially varied degradation of biomaterials.

Conflict of Interest

The University of Birmingham and S14 Implants are beneficiaries of the support by the European Commission under the 7th Framework Programme (Grant agreement no.: 604935). No employees of S14 Implants were involved in this study and no benefit of any kind will be received either directly or indirectly by the author(s).

References

[1] A.A. John, A.P. Subramanian, M. V. Vellayappan, A. Balaji, S.K. Jaganathan, H. Mohandas, T. Paramalinggam, E. Supriyanto, M. Yusof, Review: physico-chemical modification as a versatile strategy for the biocompatibility enhancement of biomaterials, RSC Adv. 5 (2015) 39232–39244. doi:10.1039/C5RA03018H.

[2] S. Ramakrishna, J. Mayer, E. Wintermantel, K.W. Leong, Biomedical applications of polymer-composite materials: a review, Compos. Sci. Technol. 61 (2001) 1189–1224. doi:10.1016/S0266-3538(00)00241-4.

[3] D.W.L. Hukins, J.C. Leahy, K.J. Mathias, Biomaterials: defining the mechanical properties of natural tissues and selection of replacement materials, J. Mater. Chem. 9 (1999) 629–636. doi:10.1039/A807411I.

[4] S.M. Kurtz, M. Steinbeck, A. Ianuzzi, A. Van Ooij, I.M. Punt, J. Isaza, E.R.S. Ross, Retrieval analysis of motion preserving spinal devices and periprosthetic tissues, SAS J. 3 (2009) 161–177. doi:10.1016/j.esas.2009.11.003.

[5] J. Jagur-Grodzinski, Biomedical application of functional polymers, React. Funct. Polym. 39 (1999) 99–138. doi:10.1016/S1381-5148(98)00054-6.

[6] J. Hartford, New Extrusion Techniques Advance Catheter Design, Med. Device Diagnostic Ind. (2013).

[7] T. Chandy, J. Van Hee, W. Nettekoven, J. Johnson, Long-term *in vitro* stability assessment of polycarbonate urethane micro catheters: resistance to oxidation and stress cracking., J. Biomed. Mater. Res. Part B Appl. Biomater. 89 (2009) 314–324. doi:10.1002/jbm.b.31218.

[8] B.M. Lawless, D.M. Espino, D.E.T. Shepherd, *In vitro* oxidative degradation of a spinal posterior dynamic stabilisation device, J. Biomed. Mater. Res. Part B Appl. Biomater. In Press (2017). doi:10.1002/jbm.b.33913.

[9] E. Cipriani, P. Bracco, S.M. Kurtz, L. Costa, M. Zanetti, *In-vivo* degradation of poly(carbonate-urethane) based spine implants., Polym. Degrad. Stab. 98 (2013) 1225–1235. doi:10.1016/j.polymdegradstab.2013.03.005.

[10] W. Schmoelz, J.F. Huber, T. Nydegger, L. Claes, H.J. Wilke, Dynamic Stabilization of the Lumbar Spine and Its Effects on Adjacent Segments An *In Vitro* Experiment, J. Spinal Disord. Tech. 16 (2003) 418–423.

[11] B.M. Lawless, S.C. Barnes, D.M. Espino, D.E.T. Shepherd, Viscoelastic properties of a spinal posterior dynamic stabilisation device, J. Mech. Behav. Biomed. Mater. 59 (2016) 519–526. doi:10.1016/j.jmbbm.2016.03.011.

[12] E.M. Christenson, J.M. Anderson, A. Hiltner, Oxidative mechanisms of poly(carbonate urethane) and poly(ether urethane) biodegradation: *In vivo* and *in vitro* correlations, J. Biomed. Mater. Res. Part A. 70 (2004) 245–255.

[13] M.C. Tanzi, D. Mantovani, P. Petrini, R. Guidoin, G. Laroche, Chemical stability of polyether urethanes versus polycarbonate urethanes, J. Biomed. Mater. Res. 36 (1997) 550–559.

[14] B.L. Wilkoff, J. Rickard, E. Tkatchouk, A.D. Padsalgikar, G. Gallagher, J. Runt, The biostability of cardiac lead insulation materials as assessed from long-term human implants, J. Biomed. Mater. Res. Part B Appl. Biomater. 104 (2015) 411–421. doi:10.1002/jbm.b.33405.

[15] M. Neukamp, C. Roeder, S.Y. Veruva, D.W. MacDonald, S.M. Kurtz, M.J. Steinbeck, *In vivo* compatibility of Dynesys spinal implants: a case series of five retrieved periprosthetic tissue samples and corresponding implants., Eur. Spine J. 24 (2015) 1074–84. doi:10.1007/s00586-014-3705-0.

[16] ISO, BS EN ISO 10993-13: Identification and quantification of degradation products from polymeric medical device, (2010) 1–28.

[17] M. Shen, K. Zhang, P. Koettig, W.C. Welch, J.M. Dawson, *In vivo* biostability of polymeric spine implants: retrieval analyses from a United States investigational

device exemption study., Eur. Spine J. 20 (2011) 1837–49. doi:10.1007/s00586-011-1812-8.

[18] A. Ianuzzi, S.M. Kurtz, W. Kane, P. Shah, R. Siskey, A. Van Ooij, R. Bindal, R. Ross, T. Lanman, K. Buttner-Janz, J. Isaza, *In Vivo* Deformation, Surface Damage, and Biostability of Retrieved Dynesys Systems, Spine (Phila Pa 1976). 35 (2010) 1310–1316.

[19] R. Hernandez, J. Weksler, A. Padsalgikar, J. Runt, *In vitro* oxidation of high polydimethylsiloxane content biomedical polyurethanes: correlation with the microstructure., J. Biomed. Mater. Res. Part A. 87 (2008) 546–56. doi:10.1002/jbm.a.31823.

[20] E.M. Christenson, J.M. Anderson, A. Hiltner, Biodegradation mechanisms of polyurethane elastomers, Corros. Eng. Sci. Technol. 42 (2007) 312–323. doi:10.1179/174327807X238909.

[21] E.M. Christenson, M. Dadsetan, M. Wiggins, J.M. Anderson, A. Hiltner, Poly(carbonate urethane) and poly(ether urethane) biodegradation: *In vivo* studies, J. Biomed. Mater. Res. Part A. 69A (2004) 407–416. doi:10.1002/jbm.a.30002.

[22] M.A. Schubert, M.J. Wiggins, J.M. Anderson, A. Hiltner, Role of oxygen in biodegradation of poly(etherurethane urea) elastomers., J. Biomed. Mater. Res. 34 (1997) 519–30.

[23] E.M. Christenson, J.M. Anderson, A. Hiltner, Antioxidant inhibition of poly(carbonate urethane) in vivo biodegradation., J. Biomed. Mater. Res. Part A. 76 (2006) 480–90. doi:10.1002/jbm.a.30506.

[24] D.K. Dempsey, C. Carranza, C.P. Chawla, P. Gray, J.H. Eoh, S. Cereceres, E.M. Cosgriff-hernandez, Comparative analysis of *in vitro* oxidative degradation of poly (carbonate urethanes) for biostability screening, J. Biomed. Mater. Res. Part A. 102 (2014) 3649–3665. doi:10.1002/jbm.a.35037.

[25] A. Simmons, A.D. Padsalgikar, L.M. Ferris, L.A. Poole-Warren, Biostability and biological performance of a PDMS-based polyurethane for controlled drug release., Biomaterials. 29 (2008) 2987–95. doi:10.1016/j.biomaterials.2008.04.007.

[26] A. Simmons, J. Hyvarinen, L. Poole-Warren, The effect of sterilisation on a poly(dimethylsiloxane)/poly(hexamethylene oxide) mixed macrodiol-based polyurethane elastomer., Biomaterials. 27 (2006) 4484–97. doi:10.1016/j.biomaterials.2006.04.017.

[27] A. Simmons, J. Hyvarinen, R.A. Odell, D.J. Martin, P.A. Gunatillake, K.R. Noble, L.A. Poole-Warren, Long-term in vivo biostability of poly(dimethylsiloxane)/poly(hexamethylene oxide) mixed macrodiol-based polyurethane elastomers., Biomaterials. 25 (2004) 4887–4900. doi:10.1016/j.biomaterials.2004.01.004.

[28] A. Mahomed, D.W.L. Hukins, S.N. Kukureka, D.E.T. Shepherd, Effect of accelerated aging on the viscoelastic properties of Elast-Eon: A polyurethane with soft poly(dimethylsiloxane) and poly(hexamethylene oxide) segments, Mater. Sci. Eng. C. 30 (2010) 1298–1303. doi:10.1016/j.msec.2010.07.014.

[29] M.J. Wiggins, B. Wilkoff, J.M. Anderson, a Hiltner, Biodegradation of polyether polyurethane inner insulation in bipolar pacemaker leads., J. Biomed. Mater. Res. 58 (2001) 302–7.

[30] S. Mukherjee, A. Gowen, A review of recent trends in polymer characterization using non-destructive vibrational spectroscopic modalities and chemical imaging, Anal. Chim. Acta. 895 (2015) 12–34. doi:10.1016/j.aca.2015.09.006.

[31] A.A. Gowen, R.M. Dorrepaal, Multivariate chemical image fusion of vibrational spectroscopic imaging modalities, Molecules. 21 (2016). doi:10.3390/molecules21070870.

[32] M.K. Kuimova, K.L. Chan, S.G. Kazarian, Chemical imaging of live cancer cells in the natural aqueous environment, Appl Spectrosc. 63 (2009) 164–171. doi:10.1366/000370209787391969.

[33] K.L.A. Chan, S.G. Kazarian, High-throughput study of poly(ethylene glycol)/ibuprofen formulations under controlled environment using FTIR imaging, J. Comb. Chem. 8 (2006) 26–31. doi:10.1021/cc050041x.

[34] S. Glassford, K.L.A. Chan, B. Byrne, S.G. Kazarian, Chemical imaging of protein adsorption and crystallization on a wettability gradient surface, Langmuir. 28 (2012) 3174–3179. doi:10.1021/la204524w.

[35] R. Dorrepaal, C. Malegori, A. Gowen, Tutorial: Time series hyperspectral image analysis, J. Near Infrared Spectrosc. 24 (2016) 89–108. doi:10.1255/jnirs.1208.

[36] ISO, BS ISO 2393: Rubber test mixes — Preparation, mixing and vulcanization — Equipment and procedures, (2014) 1–34.

[37] ASTM, ASTM D1708: Standard Test Method for Tensile Properties of Plastics by Use of Microtensile Specimens, ASTM. (2013) 1–5. doi:10.1520/D1708-13.

[38] A. Padsalgikar, E. Cosgriff-Hernandez, G. Gallagher, T. Touchet, C. Iacob, L. Mellin, A. Norlin-weissenrieder, J. Runt, Limitations of predicting *in vivo* biostability of multiphase polyurethane elastomers using temperature-accelerated degradation testing, J. Biomed. Mater. Res. Part B Appl. Biomater. 103 (2015) 159–168. doi:10.1002/jbm.b.33161.

[39] Y. Wu, C. Sellitti, J.M. Anderson, A. Hiltner, G.A. Lodoen, C.R. Payet, An FTIR-ATR Investigation of *In Vivo* Poly(ether urethane) Degradation, J. Appl. Polym. Sci. 46 (1992) 201–211.

[40] U. Trommsdorff, D. Zurbrugg, T.M. Stoll, In-vivo degradation of polycarbonate-urethane with and without contact to an abscess, in: 7th World Biomater. Congr., Sydney, Australia, 2004.